A&A 483, 847–855 (2008)
DOI: 10.1051/0004-6361:20078677

Astronomy & Astrophysics

Early emission of rising optical afterglows: the case of GRB 060904B and GRB 070420⋆

A. Klotz[1,2], B. Gendre[3,4], G. Stratta[5], A. Galli[3,6], A. Corsi[3], B. Preger[5], S. Cutini[5,7], A. Pélangeon[8], J. L. Atteia[8], M. Boër[1], and L. Piro[3]

[1] Observatoire de Haute-Provence, 04870 Saint Michel l'Observatoire, France
[2] CESR, Observatoire Midi-Pyrénées, CNRS, Université de Toulouse, BP 4346, 31028 Toulouse Cedex 04, France
e-mail: klotz@cesr.fr
[3] Istituto di Astrofisica Spaziale e Fisica Cosmica, Sede di Roma, INAF, via Fosso del Cavaliere 100, 00133 Roma, Italy
[4] University degli Studi di Milano–Bicocca, Piazza dell'Ateneo Nuovo, 20126, Milano, Italy
[5] ASI Science Data Center (ASDC), via G. Galilei, 00044 Frascati, Italy⋆⋆
[6] INFN-Trieste, Padriciano 99, 34012 Trieste, Italy
[7] Università di Perugia, Dipartimento di fisica, viale A. Pascoli, 06123 Perugia, Italy
[8] LATT, Observatoire Midi-Pyrénées, CNRS, Université de Toulouse, 14 avenue E. Belin, 31400 Toulouse, France

Received 14 September 2007 / Accepted 8 February 2008

ABSTRACT

Aims. We present the time-resolved optical emission of gamma-ray bursts GRB 060904B and GRB 070420 during their prompt and early afterglow phases.
Methods. We used time resolved photometry from optical data taken by the TAROT telescope and time resolved spectroscopy at high energies from the *Swift* spacecraft instrument.
Results. The optical emissions of both GRBs are found to increase from the end of the prompt phase, passing to a maximum of brightness at $t_{\rm peak}$ = 9.2 min and 3.3 min for GRB 060904B and GRB 070420 respectively and then decrease. GRB 060904B presents a large optical plateau and a very large X-ray flare. We argue that the very large X-flare occurring near $t_{\rm peak}$ is produced by an extended internal engine activity and is only a coincidence with the optical emission. GRB 070420 observations would support this idea because there was no X-flare during the optical peak. The nature of the optical plateau of GRB 060904B is less clear and might be related to the late energy injection.

Key words. gamma ray : bursts

1. Introduction

Since the discovery of Gamma-Ray Burst (GRB) X-ray afterglows, in 1997 (Costa et al. 1997), it has been possible to obtain a precise burst localization that allows the follow-up of GRBs from radio to X-ray (Wijers & Galama 1999). From that date, tens of GRB optical afterglows have been detected by ground-based rapid response telescopes. The launch of the *Swift* satellite, in late 2004 (Gehrels et al. 2004) has increased the usefulness of robotic telescopes. In fact, the capability of *Swift* to alert other observatories within seconds after the burst, and then re-point quickly on the burst position has allowed us to significantly increase the number of successful afterglow optical detections and to perform early optical observations. The large amount of data collected during these years has shown that during the first phases (a few hundreds of seconds) the optical emission can be as bright as $m_V \sim$ 14–17 before decreasing as $F(t) \propto t^{-\alpha}\nu^{-\beta}$, with $\alpha \sim$ 1.1–1.7 (Fox 2005; Berger et al. 2005; De Pasquale et al. 2006; Gendre et al. 2006). Several events were observed optically during the prompt phase[1], e.g. GRB 990123 (Akerlof et al. 1999), GRB 041219A (Vestrand et al. 2006), GRB 050401 (Rykoff et al. 2005), GRB 050904 (Boër et al. 2006) or GRB 060111B (Klotz et al. 2006b). In some cases the optical and γ-ray prompt emissions appeared correlated (e.g. GRB 041219A) and are likely produced by internal shocks generated by variations in the energy ejection due to the central engine (Vestrand et al. 2006). In other cases (e.g. GRB 990123) the optical prompt emission is highly variable and not correlated with the γ-ray one; they can be produced by different source regions (i.e. internal and reverse shocks respectively), and/or by different emission mechanisms (Inverse Compton and synchrotron) (Akerlof et al. 1999).

Early optical afterglow data play a role in obtaining information on the physics of the central engine, and possibly in constraining the initial Lorentz factor of the fireball (e.g. Zhang et al. 2003). However, the beginning of the optical afterglow emission is often missed either because it occurs before the first observations are completed, or because it is hidden by the high brightness of an optical flash that sometimes occurs when the GRB is still active (*e.g* GRB 060111B in Klotz et al. 2006b). Sometimes, the optical afterglow takes a few minutes to reach its maximum and rapid response optical telescopes are able to

⋆ Based on observations performed with TAROT at the Calern/OCA and La Silla/ESO observatories, GCN data archive and *Swift* public data archive.
⋆⋆ INAF personnel resident at ASDC under ASI contract 1/024/05/0.

[1] We call "prompt phase" the period during which *Swift*-BAT detected the high energy emission defined by the T_{90} duration.

record the rise of the light curve. For example this is the case of GRB 060418 and GRB 060607A (Molinari et al. 2007), which allowed investigators to constrain the initial fireball Lorentz factor to $\Gamma_0 \sim 400$.

In this paper we report the early optical observations from 23 s to 43 min of GRB 060904B and from 40 s to 18 min of GRB 070420 performed with the TAROT robotic observatories. These two GRBs have an optical afterglow that reaches a maximum hundreds of seconds after the GRB. We compare early simultaneous optical, X-ray and γ-ray data to address the question of the relation between optical and high energy emissions in the first minute after the GRB.

1.1. GRB060904B

GRB 060904B was detected on September 4th, 2006 at 02:31:03 UT by the BAT instrument on the *Swift* spacecraft (trigger = 228 006, Grupe et al. 2006). This GRB is a double–peak event (Markwardt et al. 2006): the BAT light curve shows an initial fast rise exponential decay pulse 9 s wide at 2 s before the BAT trigger (hereafter $t_{\rm trig}$) followed by a second, weaker peak detected within the 15–25 keV range, starting at $t_{\rm trig}$ + 120 s, peaking at $t_{\rm trig}$+155 s and finishing at $t_{\rm trig}$ + 220 s. T_{90} (15–350 keV) is 192 ± 5 s. *Swift*-XRT observations began at $t_{\rm trig}$ + 69 s. The X-ray light curve displays a shallow emission during the gamma emission, followed by a huge flare. Optical ground follow-up began very early when the gamma emission was still active: ROTSE-IIIc (Rykoff et al. 2006) detected a source at RA = $03^{\rm h}52^{\rm m}50.52^{\rm s}$ Dec = $-00°43'30.85''$ (J2000,0) with R = 17.3 at $t_{\rm trig}$ + 18.5 s. Klotz et al. (2006a) reported a brightening of the optical transient reaching a peak of brightness $R \sim 17$ near $t_{\rm trig}$ + 400 s. Optical spectroscopy was performed with VLT + FORS1 (Fugazza et al. 2006), at $t_{\rm trig}$+5.15 h observing several metallic absorption lines at z = 0.703. Grupe et al. (2006) mentioned that *Swift*-UVOT detected the afterglow in a finding chart exposure of 246 s with the V filter started 70 s after the BAT trigger. According to Schlegel et al. (1998) galactic extinction is $E(B-V) = 0.172$ thus implying (assuming $R_V = 3.1$) $A_B = 0.74$, $A_V = 0.57$ and $A_R = 0.46$.

1.2. GRB070420

GRB 070420 was detected on April 20th, 2007 at 06:18:13 UT by the *Swift*-BAT instrument (trigger = 276321, Stamatikos et al. 2007a). *Swift* instrument analysis was reported by Stamatikos et al. (2007b) providing celestial coordinates from UVOT at RA = $08^{\rm h}04^{\rm m}55.17^{\rm s}$ Dec = $-45°33'20''$ (J2000,0). The BAT light curve shows a slow rise that began 50 s before the trigger. T_{90} (15–350 keV) is 77 ± 4 s. *Swift*-XRT observations began at $t_{\rm trig}$ + 99 s. The X-ray light curve displays a steep decay between $t_{\rm trig}$ + 106 and $t_{\rm trig}$ + 300 s. Then, a plateau occurred until at least $t_{\rm trig}$ + 2000 s before a decay until at least few 10^4 s. No X-flare was detected. D'Avanzo et al. (2007) observed the transient at $H = 13.1 \pm 0.2$ with the REM telescope. From high energy spectral properties delivered by the KONUS experiment, Pélangeon & Atteia (2007) computed a pseudo-redshift $pz = 1.56 \pm 0.35$. UVOT detection in the U band (Immler et al. 2007) confirms the low redshift of the burst. According to Schlegel et al. (1998) galactic extinction is $E(B-V) = 0.50$. Assuming $R_V = 3.1$, the extinctions are thus $A_B = 2.18$, $A_V = 1.63$, $A_R = 1.33$, $A_H = 0.29$.

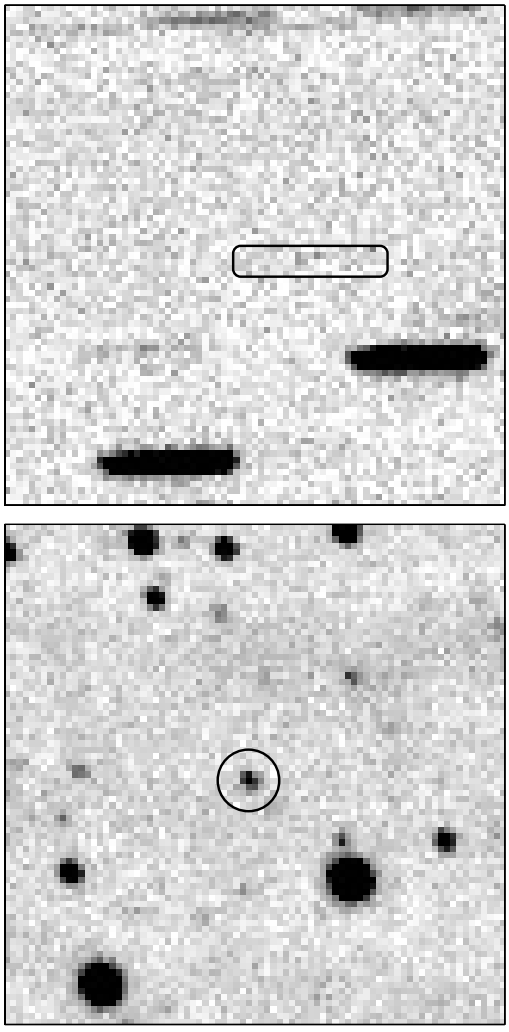

Fig. 1. GRB 060904B. *Top*: this image was taken between 23 s and 83 s after the GRB trigger. The hour angle velocity was adapted to obtain stars as trails of ~20 pixel length during the 60 s exposure. The theoretical position of the GRB trail is indicated by the rectangle. A cluster of 4 pixels is present near the center of the rectangle but is considered as noisy pixels or "cosmic" trace rather than an optical flash (see text). *Bottom*: sum of images taken by TAROT in diurnal motion mode. The optical transient position is indicated by the circle. The image size is 7 arcmin, North is up, East left.

2. TAROT observations

TAROT are two fully autonomous 25 cm aperture telescopes installed at Calern observatory (Observatoire de la Côte d'Azur – France) and at La Silla observatory (European Southern Observatory – Chile). These telescopes are devoted to very early observations of GRB optical counterparts. A technical description can be found in Bringer et al. (2001). GRB 060904B was observed with TAROT Calern and GRB 070420 with TAROT La Silla.

When the notice is received, the first image is an unfiltered 60 s exposure taken in drift mode (see Figs. 1 and 2 top, described in Klotz et al. 2006b). For each GRB, the image began during the prompt phase with a drift velocity of 3 s/pixel. Successive images were tracked on the diurnal motion. A first series of five unfiltered (hereafter filter C) 30 s images was followed by four series of three 90 s images filtered C–C–R respectively. Finally, series of three 180 s images were taken with the

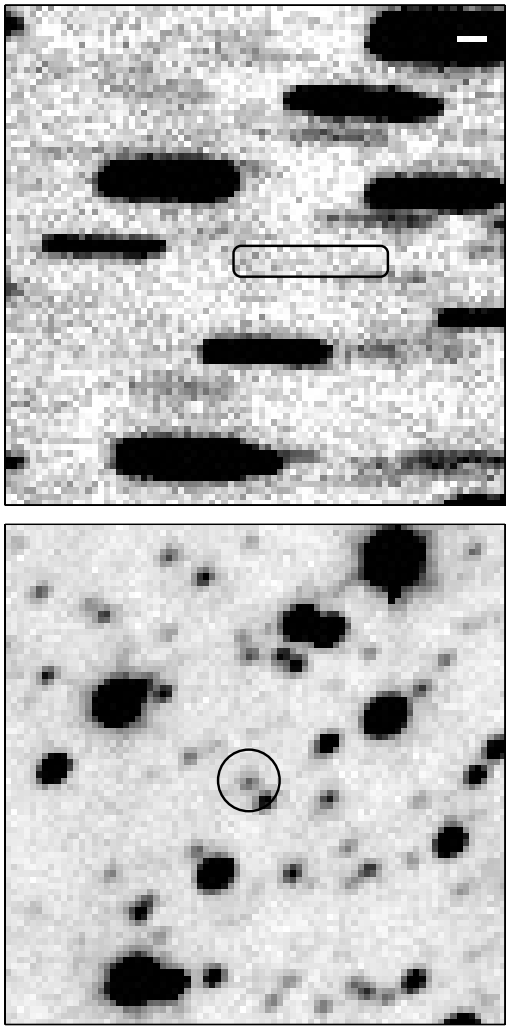

Fig. 2. GRB 070420. *Top*: this image was taken between 34 s and 94 s after the GRB trigger in drift mode (see Fig. 1). Three nearby stars (see Sect. 2.1) have been subtracted. The position of the GRB trail is indicated by the rectangle. A group of faint lightened pixels is present in the first third of the rectangle but we cannot conclude on its significance. *Bottom*: Sum of images taken by TAROT in diurnal motion mode. The optical transient position is indicated by the circle (nearby stars are not subtracted). The image size is 7 arcmin, North is up, East left.

same filter alternance. In the GRB 060904B case, the drift image began at $t_{\rm trig}+23$ s and entirely spans the prompt phase (that extends until 220 s after the trigger). Dawn arrived 43 min after the trigger and observations were stopped. For GRB 070420, the drift image began at $t_{\rm trig}$ + 34 s. The field elevation decreased from 8 degrees above horizon to 5 degrees at the end of observations. Only the first 18 minutes of the event were recorded. Logs of observations are included in Tables 1 and 2.

2.1. Image processing

Photometry was performed using Point Spread Function (PSF) fitting taking a nearby star image as the PSF: USNO-B1 0892-0038669 for GRB 060904B and USNO-B1 0444-0107368 for GRB 070420. C magnitudes were rescaled in the R band considering the absence of dramatic spectral changes in the optical range. In the case of GRB 070420, three stars lie very close to the GRB location: USNO-B1 0444-0107222 (5″, R = 17.3), USNO-B1 0444-0107218 (7″, R = 17.6), USNO-B1 0444-0107203 (13″, R = 15.6). We subtracted these stars using the PSF of USNO-B1 0444-0107368 (R = 13.3) before the PSF fitting of the GRB. Tables 1 and 2 give photometric results of both GRBs from TAROT and other useful measurements published in GCN Circulars.

2.2. Trailed images

At the GRB 060904B position (Fig. 1, top), no trail is detected at $R < 17.2$ except for a small cluster of 4 pixels near $t_{\rm trig}$ + 42.8 s. We first considered it as a possible optical flash associated with the GRB (Klotz et al. 2006a). The punctual shape implies that its duration is less than 3 s (the time sampling of the trail) corresponding to $R < 15.9$. Rykoff (private communication) provided us with a series of 5 s exposures obtained with ROTSE-III telescopes. One of these images was taken between $t_{\rm trig}+42.6$ s and $t_{\rm trig}$ + 47.6 s. It shows no object brighter than R = 16.7. As a consequence, we do not confirm this flash to be real. From a statistical point of view, the signal to noise ratio (S/N) of the four involved pixels are : 1.0, 2.0, 2.7, 2.8. Considering a Gaussian noise distribution of the sky background, simultaneous values higher than the corresponding S/N is $\sim 10^{-6}$ for four contiguous pixels. This excludes a natural background fluctuation. Thus, it is probably an artifact (e.g. a cosmic trace). We took this into account when we computed limiting magnitudes (see Fig. 3). From TAROT and ROTSE-III data, we conclude that the optical emission was $R > 17.2$ during the prompt emission, except during $t_{\rm trig}$ + 41.3 s to $t_{\rm trig}$ + 44.3 s where it was $R > 15.9$.

In the case of GRB 070420 (Fig. 2 top), a very faint trace is present at the beginning of the theoretical place of the trail but the signal to noise ratio is lower than 3, preventing any conclusion.

2.3. The optical afterglow of GRB 060904B

The optical light-curve of GRB 060904B is shown in Fig. 3. Before the end of the prompt phase, the optical emission rose with a slope $\alpha_1 = -0.82$ between $t_{\rm trig}$ + 90 s and $t_{\rm trig}$ + 550 s reaching R = 16.8 at $t_{\rm trig}+550$ s. Then, the flux decreased with a slope $\alpha_2 = 1.0$ down to R = 17.8 at $t_{\rm trig}$ + 1270 s. From this date, the flux remained at a constant level until the end of the available early observations ($t_{\rm trig}$ + 49.8 min). Late observations obtained 15 hs after the trigger imply a late decay index of $\alpha_3 = 1.03$ in the range $t_{\rm trig}$ + [50 min–1.9 day].

Interpolating R, B and V magnitude measurements, we deduced $(B-R)$ at several dates (Table 3). At z = 0.703 (redshift of GRB 060904B) the color indexes are not affected by the Lyman-α cut-off (Roming et al. 1999). According to Simon et al. (1998), $(B-R)_0 = 0.8 \pm 0.3$ for typical early afterglows. The observed $(B-R)$ values of GRB 060904B, corrected for the galactic extinction, are compatible with a weak local extinction. Cobb & Bailyn (2007) obtained data in the *JHK* bands during the late afterglow phase. They confirm a weak extinction. From published optical and near infrared data obtained during the late afterglow phase, Kann et al. (2008) derived the intrinsic extinction $A_V = 0.44 \pm 0.05$ using a Small Magellanic Cloud dust model.

2.4. The optical afterglow of GRB 070420

The optical light-curve of GRB 070420 is shown in Fig. 4. After the end of the prompt phase, optical emission had risen at a rate $\alpha_1 = -1.26$. This rising rate is compatible with V band data

Table 1. Log of the optical measurements of GRB 060904B from TAROT and GCN Circulars. T are seconds since t_{trig}. C magnitudes of TAROT images were translated to the R photometric band by an appropriate offset. Errors Δmag are 2σ for TAROT data.

T_{start}	T_{end}	mag.	Δmag.	GCNC Ref.
18.5	23.5	R17.30	0.10	5504
23.0	41.3	$C > 17.2$		TAROT
41.3	44.3	$C > 15.9$		TAROT
44.3	86.0	$C > 17.2$		TAROT
57.8	147.8	R 18.21	0.02	5511
90.8	120.8	C 18.38	0.47	TAROT
128.1	157.4	C 17.76	0.32	TAROT
164.1	194.7	C 17.99	0.35	TAROT
71.0	316.0	V 18.64	0.30	5519
200.7	230.7	C 17.61	0.26	TAROT
237.8	267.9	C 17.15	0.20	TAROT
177.8	358.8	B 18.32	0.04	5511
283.5	373.5	C 17.31	0.13	TAROT
380.1	470.1	C 17.02	0.11	TAROT
387.8	477.8	R 17.01	0.02	5511
502.0	527.0	R 16.90	0.12	5541
479.7	569.7	R 16.78	0.09	TAROT
526.2	526.2	R 16.75	0.02	5524
597.6	597.6	R 16.86	0.03	5524
507.8	687.8	B 17.51	0.04	5511
578.0	668.0	C 16.94	0.11	TAROT
664.2	664.2	R 16.99	0.03	5524
653.0	678.0	R 17.09	0.16	5541
674.7	765.3	C 17.06	0.11	TAROT
735.0	735.0	R 17.05	0.04	5524
718.8	808.8	R 17.11	0.02	5511
784.8	784.8	R 17.22	0.05	5524
777.0	803.0	R 17.24	0.19	5541
774.3	864.3	R 17.22	0.14	TAROT
874.8	874.8	R 17.34	0.06	5524
889.0	914.0	R 17.36	0.17	5541
881.1	971.1	C 17.52	0.17	TAROT
838.8	1018.8	B 18.56	0.04	5511
1014.0	1014.0	R 17.48	0.09	5524
1004.0	1029.0	R 17.44	0.14	5541
978.3	1067.7	C 17.54	0.16	TAROT
1083.0	1083.0	R 17.50	0.09	5524
1073.0	1098.0	R 17.58	0.14	5541
1048.8	1138.8	R 17.79	0.02	5511
1077.3	1167.3	R 17.34	0.16	TAROT
1153.8	1153.8	R 17.64	0.10	5524
1175.6	1265.6	C 17.56	0.16	TAROT
1168.8	1348.8	B 18.81	0.04	5511
1272.8	1362.3	C 17.93	0.22	TAROT
1371.3	1461.8	R 17.86	0.24	TAROT
1378.8	1468.8	R 18.21	0.02	5511
1466.0	1491.0	R 17.70	0.22	5541
1505.0	1530.0	R 17.75	0.20	5541
1479.3	1659.8	C 17.63	0.17	TAROT
1669.0	1694.0	R 17.94	0.18	5541
1665.8	1846.5	C 17.96	0.20	TAROT
1712.8	1802.8	R 17.66	0.02	5511
1751.0	1776.0	R 17.79	0.21	5541
1802.0	1827.0	R 17.89	0.14	5541
1854.8	2034.8	R 17.67	0.17	TAROT
2044.5	2223.8	C 17.78	0.20	TAROT
2231.1	2410.4	C 17.96	0.18	TAROT
2242.8	2422.8	R 17.78	0.02	5511
2419.5	2600.0	R 17.61	0.22	TAROT
2538.8	2718.8	R 17.79	0.02	5511
2805.8	2985.8	R 17.99	0.02	5511
56 592.0	56 592.0	R 21.40	0.20	5548
76 529.4	77 969.4	R 21.63	0.18	5741
86 477.4	87 377.4	R 21.75	0.11	5526
87 514.2	88 414.2	R 21.74	0.12	5526
89 415.0	90 315.0	R 21.80	0.20	5526
162 531.0	16 3731.0	R 22.40	0.30	5741

Table 2. Log of the optical measurements of GRB 070420 from TAROT and GCN Circulars. Columns and units are the same as Table 1.

T_{start}	T_{end}	mag.	Δmag.	GCNC Ref.
39.9	48.9	$C > 16.75$		TAROT
48.9	57.3	$C > 16.45$		TAROT
57.3	65.7	$C > 16.25$		TAROT
65.7	74.7	$C > 16.75$		TAROT
74.7	83.1	$C > 16.75$		TAROT
83.1	91.5	$C > 16.75$		TAROT
90.0	100.0	V 17.90	0.10	6336
101.1	131.0	C 16.64	0.18	TAROT
137.6	166.4	C 16.46	0.13	TAROT
109.0	208.0	V 17.40	0.10	6336
173.1	203.1	C 16.03	0.11	TAROT
296.1	386.1	C 16.38	0.12	TAROT
392.1	482.0	C 16.73	0.17	TAROT
491.6	582.3	R 16.84	0.23	TAROT
590.0	680.0	C 17.05	0.31	TAROT
693.0	703.0	B 18.80	0.10	6336
686.0	776.0	C 17.05	0.26	TAROT
890.0	980.1	C 17.50	0.41	TAROT
986.1	1075.5	C 17.65	0.47	TAROT
10 530.0	11 154.0	R 19.70	0.40	6334
12 678.0	13 308.0	I 19.30	0.50	6334

Table 3. Color indexes for GRB 060904B. T_{mean} is the time since t_{trig} when the color indice is measured. T_{mean} is expressed in seconds. Column "mag." is not corrected for galactic extinction. Column "dereddened" is the color corrected by the galactic extinction.

T_{mean}	Color	mag.	Deredened	Uncert.	Remarks
193	$V-R$	1.0	0.89	0.3	bad sampling
268	$B-R$	0.93	0.65	0.04	optical rising
598	$B-R$	0.72	0.44	0.04	close to the top of the bump
929	$B-R$	1.10	0.82	0.04	optical decreasing
1259	$B-R$	1.0	0.72	0.04	optical shallowing
4425	$B-R$	0.58	0.30	0.15	late afterglow
4831	$V-R$	0.64	0.53	0.36	late afterglow
5649	$B-R$	0.88	0.60	0.28	late afterglow

provided by UVOT (Immler et al. 2007). The optical data show a temporal gap at the maximum of the emission (due to a technical problem). Extrapolating the data, we estimate the peak of emission to occur near t_{trig} + 3.3 min with a magnitude of $R = 15.9$. Then the flux decreased at a rate of $\alpha_2 = 0.89$ to $R = 17.6$ at t_{trig} + 17.2 min. Later observations obtained 3 hours after the trigger are compatible with this decay. If we set the t_{trig} time to the onset of the start of the BAT emission (50 s earlier than the trigger time) we obtain $\alpha_1 = -1.69$ and $\alpha_2 = +0.91$.

Interpolating R and some other band magnitude measurements we deduced color indexes at several epochs (Table 4). At t_{trig} + 95 sdec, $(V - R) = +0.5$ (corrected for galactic extinction). At t_{trig} + 698 s, during the optical decreasing phase, $(B - R) = +0.85$.

3. High energy observations

3.1. BAT analysis of GRB 060904B

We have performed temporal and spectral analysis of the BAT data for GRB 060904B. Figure 5 shows the light curve in the 15–25 and 100–150 keV ranges: the numbered vertical columns

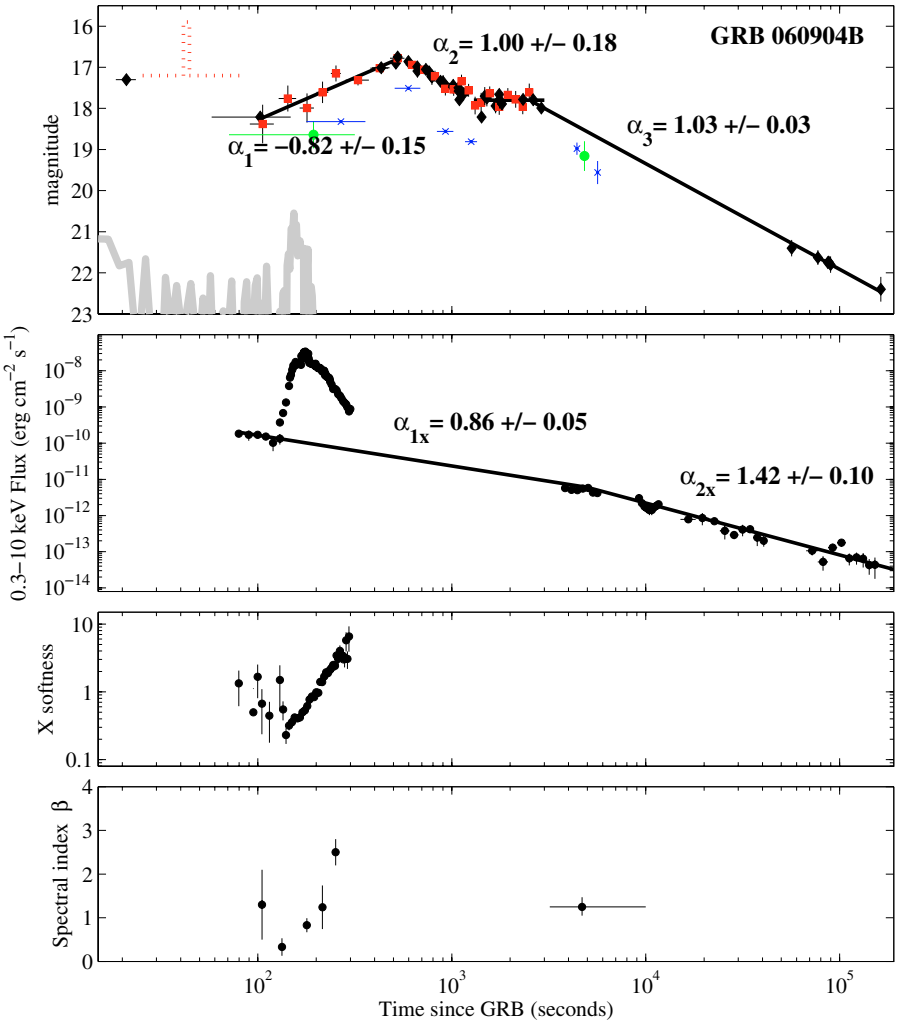

Fig. 3. Time resolved parameters of GRB 060904B. *Top panel*: optical light-curve. Data are provided from Table 1. Red squares are TAROT data (plus the limiting magnitude during 23 s to 83 s indicated by the dotted line). Black diamonds are *R* measurements of other observatories. Green disk and blue x are from the literature for the *V* and *B* band respectively. The BAT light curve is displayed as the light gray curve offset arbitrarily. Fits are based on the flux law: $f(t) \propto t^{-\alpha}$. *Second panel*: X-ray light-curve from XRT data. The count rate has been converted to flux units using the best fit spectral model of late X-ray afterglow (to avoid spurious features due to the large spectral variations observed during the flare). Third panel: softness ratio defined by (0.3–1.5 keV)/(1.5–10 keV). *Bottom panel*: X-ray band spectral index.

Table 4. Color indexes for GRB 070420. See column descriptions in Table 3.

T_{mean}	Color	mag.	Deredened	Uncert.	Remarks
95	$V-R$	0.8	0.5	0.2	optical rising
300	$R-H$	3.15	2.1	0.1	optical decreasing
698	$B-R$	1.7	0.85	0.1	optical decreasing

refer to the TAROT observation periods with a detected optical source. No high energy precursor is detectable up to t_{trip} – 200 s. No signal was detected by BAT during the first TAROT observation (window number 1), whereas observations number 2 and 3 cover the second and much fainter peak in the high energy light curve. In order to obtain broad band time-resolved spectra for GRB 060904B, we performed spectral analysis of the BAT data in three different epochs: the main peak, visible only by BAT (from t_{trip} – 5s to t_{trip} + 25 s), the rise of the second peak (from t_{trig} + 123.9 s to t_{trig} + 159.9 s), and the decay of the second peak (from t_{trig} + 159.9 s to t_{trig} + 197.1 s). The second and third time intervals are slightly longer than (but centered on) the two corresponding TAROT observations (t_{trig} + [128.1–157.4] s and t_{trig} + [164.1–194.7] s respectively). This choice was made in order to increase the signal to noise ratio and thus the quality of the obtained spectra while maintaining a good simultaneity of the observations.

The 15–150 keV energy spectra during all the 2 and 3 TAROT epochs are well fitted by a simple power law model. We find clear evidence of spectral softening through the three epochs: the photon index is in fact $\Gamma_1 = 1.35 \pm 0.1$ during the main peak, $\Gamma_2 = 2.16 \pm 0.3$ during observation number 2 and $\Gamma_3 = 2.34 \pm 0.4$ during observation number 3. The spectral softening is also confirmed by a comparison of the light curves in the 15–25 keV and 100–150 keV energy bands (Fig. 5).

The fluence in the first peak is 1.22×10^{-6} erg cm^{-2}, in the second peak (observations 2 and 3 together) 3.68×10^{-7} erg cm^{-2} for a total fluence of 1.6×10^{-6} erg cm^{-2}.

3.2. XRT analysis of GRB 060904B

The XRT began observing 69 s after the BAT trigger (Grupe et al. 2006). The data were processed using the ftools version 6.1.2. Data taken in *window timing* mode suffered from severe pile-up during the flare and were corrected using the prescriptions indicated in Romano et al. (2006). We used a rectangle box extraction region excluding 2 central pixels for the time intervals between t_{trig} + 145 s and t_{trig} + 166 s and between t_{trig} + 182.9 s and t_{trig} + 237.3 s, and 5 central pixels for the time interval between t_{trig} + 166.0 s and t_{trig} + 182.9 s. The extraction region was 50 pixel large. We corrected for the effects induced by a bad column and the pile-up excluded region located within the extraction region by estimating from the Ancillary Response

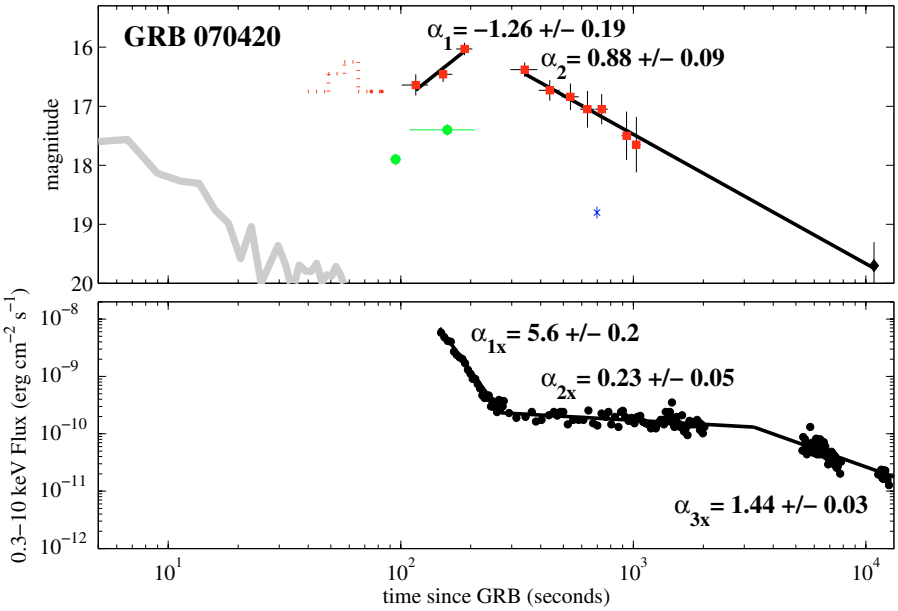

Fig. 4. Global light-curves of GRB 070420. Data are from Table 2. Red squares are TAROT data (plus the limiting magnitude during 40 s to 91 s indicated by the dotted line). Black diamonds are *R* measurements of other observatories. The green disk and blue x are from the literature for the *V* and *B* band respectively. The BAT light curve is displayed as the light gray curve.

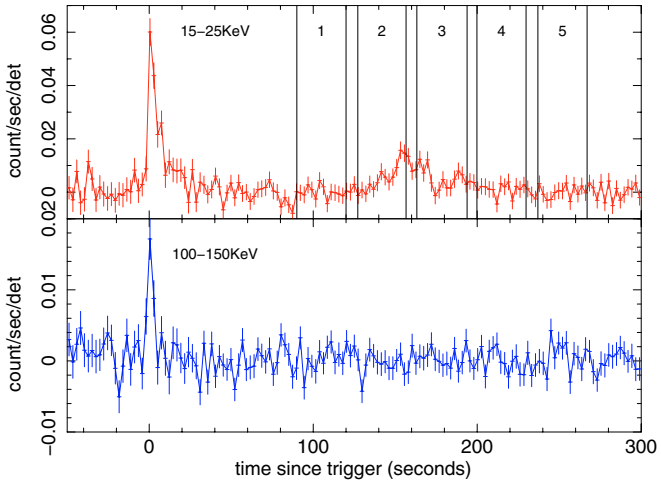

Fig. 5. BAT light curves at different energy ranges for GRB 060904B. The second peak near $t_{\rm trig}$ + 160 s is only visible in the softest energy band. The vertical lines define the 5 intervals coincident with the TAROT observations.

File the fraction of lost counts, and corrected all count rates for this loss. The light curve was extracted within the 0.3–10.0 keV band and rebinned in order to obtain at least 25 counts per bin. All decay indexes indicated below are derived by fiting power laws using the χ^2 statistic. As the 0.3–2.0 keV range is not free from absorption, we prefered, for comparison with other works, to produce the figures using the standard 2.0–10.0 keV band (free of absorption). We thus converted all 0.3–10.0 keV count rates into a standard 2.0–10.0 keV flux by using the appropriate mean conversion factor derived from the spectral analysis (see below). The light curve shows an initial shallow decay between 77.3 s and ~138 s followed by a giant flare (temporal index rise $=-17.83 \pm 0.02$, temporal decay index $= 6.1 \pm 0.4$) with a duration of 490 s (see Fig. 3). This flare has a 0.3–10.0 keV mean flux of 2.2×10^{-9} erg s^{-1} cm^{-2} and a total fluence of 8.8×10^{-7} erg cm^{-2}. The data feature a temporal gap between ~300 and ~3500 s. However, the data taken before and after the flare are consistent with a continuous and smooth power law decay with index $\alpha_{1x} = 0.86 \pm 0.05$ followed by a break near $(5 \pm 1) \times 10^3$ s and a final decay with index $\alpha_{2x} = 1.42 \pm 0.1$. We do not find evidence of a plateau phase in X-ray.

We extracted the XRT spectra during each TAROT temporal bin (see Table 5), plus a global spectrum in order to derive a mean count-to-flux conversion factor for light curve conversions. All spectra were rebinned in order to include 20 net counts within each bin, and fit using the χ^2 statistic. The spectral model was composed of a power law continuum absorbed by our galaxy (Galactic hydrogen column density fixed at 1.21×10^{21} cm^{-2}, Dickey & Lockman 1990) and by the host galaxy at $z = 0.703$. When possible, we fit the BAT and XRT spectra together. During the flare, the spectrum softens but more interestingly the foreground hydrogen column increases during the rising phase of the flare and then it decreases. This is a quite uncommon behavior and we interpret it as an artificial effect of a wrong assumption on the intrinsic spectral model. A Band model or cut-off power law provides a more realistic behavior (see Table 5), with a constant extragalactic absorption of $N_H = (8 \pm 2) \times 10^{21}$ H cm^{-2} (at $z = 0.703$), and an hard-to-soft behavior, characteristic of prompt related emission. Very similar results have been obtained in the past for another giant X-ray flare associated with GRB 050502B (Falcone et al. 2006). The difference with GRB 060904B is that no rising optical afterglow was detected during the flare (or after). The late XRT data of GRB 060904B (from ~3700 to ~6000 s) are compatible with a simple absorbed power law (extragalactic $N_H = (5 \pm 2) \times 10^{21}$ H cm^{-2}, $\beta = 1.3 \pm 0.3$, $\chi^2_\nu = 1.21$, 19 d.o.f.). Compared to the spectral index found for the early XRT data (before the giant X-ray flare, see Table 5), no significant changes are observed within the errors.

3.3. BAT analysis of GRB 070420

We have performed temporal and spectral analysis of the BAT data for GRB 070420. The light curve, visible in Fig. 6 in the 15–350 keV energy range, shows a slow rise beginning about 50 s before the BAT trigger, then a multi-peaked structure and finally a gradual decay ending about 100 s after the trigger. Again, the vertical columns refer to the TAROT observing windows, but for this GRB no signal was detected by BAT that could be used to derive simultaneous broad band spectra at those epochs.

Table 5. Spectral analysis of GRB 060904B. We indicate only the best fit models (*top panel*, a cut-off power law; *bottom panel*, a Band model). Column Bin refers to the TAROT measurements defined in Sect. 3.1 and reported in Fig. 5. Bins 1, 4, and 5 are XRT data only, while bins 2 and 3 are XRT and BAT data fit together. Values between parentheses are set to the value indicated. Extragalactic absorption is computed in the GRB rest frame. The two spectral indexes of the Band function are given as low energy spectral index first, high energy spectral index after. Several values are not constrained by the fit (the E_0 values for bins 1 and 5 with a cut-off power law). All errors are given at the 90% confidence level. When applicable, upper limits are given at the 95% confidence level.

Epoch (seconds since trigger)	Bin	Spectral index	E_0 (keV)	Extragalactic absorption (10^{22} cm^{-2})	χ^2_ν	d.o.f.
90.8–120.8	1	1.3 ± 0.8	–	(0.78)	0.92	1
127.2–156.6	2	0.3 ± 0.2	$37.9^{+36.6}_{-14.5}$	0.8 ± 0.5	1.08	28
163.2–193.8	3	0.8 ± 0.2	$13.2^{+7.0}_{-4.1}$	0.8 ± 0.2	1.18	119
199.8–229.8	4	1.2 ± 0.5	$6.8^{+13.4}_{-3.8}$	0.6 ± 0.2	0.93	61
237.0–267.0	5	2.5 ± 0.3	–	0.8 ± 0.2	1.09	42
127.2–156.6		0.3 ± 0.2	$39.6^{+35.7}_{-15.4}$	0.8 ± 0.5	1.12	27
		>6.84				
163.2–193.8		0.6 ± 0.4	$5.7^{+4.2}_{-2.9}$	0.7 ± 0.2	1.05	118
		1.8 ± 0.3				
199.8–229.8		1.3 ± 0.5	$7.4^{+4.1}_{-3.9}$	0.6 ± 0.1	0.95	60
		–				
237.0–267.0		–	<3.59	0.7 ± 0.2	1.11	41
		2.4 ± 0.2				

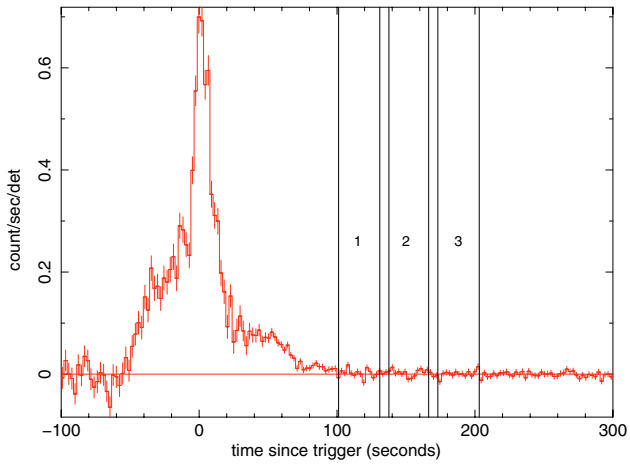

Fig. 6. BAT total light curve (15–350 keV) for GRB 070420. The vertical lines define the 3 intervals coincident with the TAROT observations. Note that a signal due to GRB 070420 is detected up to ~50 s before the trigger time.

We have therefore performed the spectral analysis using the signal integrated over the BAT T_{90}: a simple power law fits the observed spectrum between 15 and 150 keV with $\Gamma = 1.54 \pm 0.06$, while the burst fluence is 1.43×10^{-5} erg cm^{-2}.

We observed no significant spectral evolution during the emission detected by BAT.

3.4. XRT analysis of GRB 070420

The XRT observation starts 99.0 s after the BAT trigger; and 159 s after the start of the gamma-ray emission (which we define as the start of the event). The 0.3–10.0 keV light curve is very smooth and features the standard "steep-flat-steep" behavior observed in the *Swift* era (O'Brien et al. 2005), with no flare superimposed (see Fig. 4). The three segments decay as $\alpha_{1x} = 5.6 \pm 0.2$, $\alpha_{2x} = 0.23 \pm 0.05$ and $\alpha_{3x} = 1.44 \pm 0.03$ respectively, with two break times of $t_{b1} = (3 \pm 1) \times 10^2$ and $t_{b2} = (3.3 \pm 0.2) \times 10^3$ s. Note that these values differ from the ones reported in Stratta et al. (2007), as the start time of the event is different (Stratta et al. 2007, used the trigger time as T_0, while we used the start of the event as T_0).

The PC data suffer from a moderate pile-up during 280.2 and ~7800 s after the trigger. The initial *window timing* data provide a good fit with a simple absorbed power law, and are consistent with no spectral variations (spectral index $\beta = 1.5 \pm 0.1$, extragalactic absorption $N_H < 1 \times 10^{20}$ H cm^{-2}, $\chi^2_\nu = 1.25$, 116 d.o.f.). The same spectral model results in a spectral index of $\beta = 1.2 \pm 0.1$ and $\beta = 0.9 \pm 0.2$ ($\chi^2_\nu = 1.30$, 50 d.o.f.) during the plateau phase and the following decay respectively. Note that the galactic hydrogen column density along the direction of the GRB is $N_H = 3.7 \times 10^{21}$ H cm^{-2}.

4. Discussion

4.1. The giant flare of GRB 060904B

Giant X-ray flares such as the one observed for GRB 060904B have also been observed for other GRBs (see Burrows et al. 2007; Chincarini et al. 2007, for a review). In particular, the giant flare associated with GRB 050502B was studied in detail by Falcone et al. (2006). Compared with the giant X-ray flare of GRB 060904B, the similarities are striking. GRB 070704 is another example of a GRB with a large X-ray flare ~300 s after the trigger (Godet & Sakamoto 2007).

First, as for GRB 050502B, we find that the spectrum of GRB 060904B during the flare cannot be fitted by a power law, unless allowing for a variable absorption. The latter shows a significant increase at the onset of the flare, followed by a decrease (which is unusual behavior). We thus modeled the spectra using a Band model and a cut-off model, finding a better explanation. The consistency with the Band model (or cutoff power law) suggests that the flare could be caused by the same mechanism powering the prompt emission, as in a late time internal shock scenario, which was suggested to explain the GRB 050502B giant flare.

The spectral and temporal analysis of the flare show other similarities with the case of GRB 050502B, such as: i) the increasing softening of the spectrum as the flare develops (see Fig. 3); ii) the hard band decaying more quickly than the soft band after the peak of the flare ; iii) the soft band having a shallower decay relative to the slope of the flare rise (see Table 6).

The temporal decay observed before the flare seems to extrapolate to 4000–5000 s after the trigger, with no evident increase in the pre-flare versus the post-flare light curve normalization. This also suggests that the X-ray flare could be produced by an additional mechanism, independent to the one generating the underlying emission. Such emission, in turn, could be interpreted as resulting from the superposition of a decaying prompt and a rising X-ray afterglow component, as proposed by Willingale et al. (2007) to interpret the typical "steep-flat-steep" behavior of *Swift* XRT light curves. In this scenario, the temporal break observed in the X-ray light curve around $(5 \pm 1) \times 10^3$ s could mark the transition from the "flat phase" to the "steep" afterglow-dominated phase. We note that the observed steepening in the X-ray light curve ($\Delta\alpha = 0.56 \pm 0.11$) is not consistent with a spectral break within a standard afterglow scenario (that would require $\alpha_{1x} - \alpha_{2x} = 0.25$) nor with

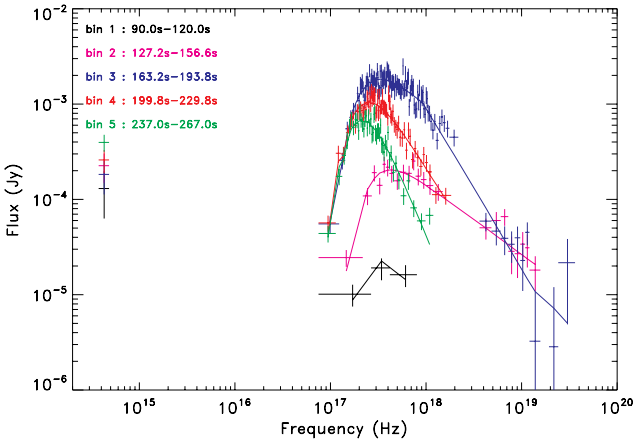

Fig. 7. Evolution of the spectral emission distribution of GRB 060904B according to the first bins corresponding to TAROT exposures. The theoretical model represented is a Band function. It is not possible to reconcile optical and X-ray data with only power-law and extinction. This argues that the optical emission has a different origin to that of the X-ray flare.

an achromatic jet break (the optical light curve seems to extrapolate without breaks from ∼3000 s to late times, see Fig. 3). In addition, the late-time ($t \gtrsim 5000$ s) optical-to-X-ray temporal and spectral indices verify (within the errors) the closure relations expected in a standard afterglow scenario, when ν_m is below the optical band and ν_c between the optical and the X-ray band (see e.g. Zhang & Meszaros 2004).

We thus conclude that the giant X-ray flare of GRB 060904B may be due to a late internal shock.

4.2. Optical rising

An optical rising has been observed for both GRB 060904B and GRB 070420. For GRB 070420, the rising occured during the X-ray steep decay (see Fig. 4). *V*-band UVOT observations (Immler et al. 2007) suggest an achromatic behavior.

Differently from the cases of GRB 050502B or GRB 070704, which had no optical counterpart, for GRB 060904B an optical emission is observed: the optical light curve rises smoothly during the whole X-ray flare, and shows a maximum after the end of the X-ray flare. One could consider the possibility that this flare is correlated with the optical rise. In fact, the broad band data suggest a temporal sequence, with a flare moving from the γ-ray band to the optical band (see Fig. 3). In such a case the X-ray and optical emissions are produced by the same mechanism (internal shock, see Sect. 4.1), with the peak of the emission moving from the BAT to optical bands. Hence, near the peak of the emission one should expect the same spectro-temporal behavior. However, the observed X-ray rise and decay temporal slopes are significantly steeper than the optical ones (see Table 6). This suggests that the optical rising and the BAT-XRT flare are not correlated. We also note that extrapolating in the optical band the best fit Band models listed in Table 5, results in an overestimation of the optical flux. We can reconcile the observed optical data with the high energy extrapolation only by invoking a strong extinction. Moreover, such extinction should increase as the flare develops, which is an unsual behavior.

A similar rise was observed in the near infrared light curves of GRB 060418 and GRB 060607A (Molinari et al. 2007), together with a simultaneous X-ray emission characterized by the presence of various flares. In these cases, the low-energy optical rise was interpreted as the peak of the afterglow emission which, in the standard thin shell case, is predicted to occur around the deceleration time $t_{\rm dec} \sim t_{\rm peak}$ (Sari & Piran 1999; Kobayashi & Zhang 2007). Up to now, only a tenth of optical afterglows have been observed sufficiently early, and time-sampled sufficiently well for the optical rising to be clearly identified. Theoretically, if the rise has to be ascribed to the beginning of the afterglow, in a standard ISM scenario the temporal index α_1 is expected to be ≤ -2 (Sari & Piran 1999), much steeper than our observed value. In the case of a fireball expanding in a wind environment, the rise could be less steep and also followed by a plateau (see e.g. Fig. 1 of Wu et al. 2003). In such a case, we would expect the late optical light curve to decrease with the same temporal index, or more steeply, than in the X-rays. However, as discussed in Sect. 4.1, if we interpret the X-ray emission at ∼5000 s as the link to the "standard" afterglow phase, then the hypothesis of an expansion in a wind environment does not agree with the late time observations. In fact, at $t \gtrsim 5000$ s, the X-ray decay is steeper than the optical one.

Table 6. Summary of temporal indixes for the optical and X-ray light curves of GRB 060904B. We report a decay with positive index and an increase with negative index.

Part	Optical index	X-ray index
Pre X-flare	n.d.	0.86 ± 0.05
X-flare rise	-0.82 ± 0.15	-17.83 ± 0.02
X-flare decay	-0.82 ± 0.15	6.1 ± 0.4
Optical Peak	0	0.86 ± 0.05
First optical decay	1.00 ± 0.18	0.86 ± 0.05
Optical plateau	0	0.86 ± 0.05
Final decay before X-break	1.03 ± 0.03	0.86 ± 0.05
Final decay after X-break	1.03 ± 0.03	1.42 ± 0.10

Other phenomena can also contribute to a late rising of the optical afterglow: i) an off axis line of sight (Granot et al. 2002) as was supposed in the case of GRB 060206 by Wozniak et al. (2006) for which the fluence was very low ($8.4 \pm 0.4 \times 10^{-7}$ erg cm^{-2} in the 15–150 keV range). This is not the case for GRB 070420 for which the fluence is exceptionally high. Moreover, in the case of an off-axis observer, the X-ray and the optical light curves must follow the same behavior, which is not the case of the two studied GRBs. ii) The circumstellar medium could be very dense and the extinction very high at the beginning of the optical afterglow, and could decrease later because of the dust destruction implied by the burst blast wave (Perna & Loeb 1998). This is probably not the case of GRB 060904B because optical emission was detected by ROTSE during the prompt emission and color indexes do not show a red excess near $t_{\rm peak}$. Optical indexes prove that the extinction was not high in both GRBs. iii) In the case of a smooth gradient of interstellar material density (Tam et al. 2005), the rise is explained by an appropriate density profile if the optical emission is below the cooling frequency (Sari et al. 1998). iv) Reverse shock emission could be invoked. In this scenario, one could interpret the optical bump of GRB 060904B as an optical flash, and the following plateau as the result of the forward shock emission adding up to the reverse shock one: see Fig. 2 of Sari & Piran (1999). However, in such a case, the extrapolated power-law behavior of both the rise and decay of the reverse shock optical emission are expected to be somewhat steeper than those observed in our case (Sari & Piran 1999; Kobayashi & Zhang 2007). v) the optical rise and decay temporal indexes of $\alpha_1 = -0.82 \pm 0.15$ and

$\alpha_2 = 1.00 \pm 0.18$, could be marginally accommodated within a standard afterglow scenario, by having the ν_m cross the optical band.

4.3. Optical plateau

Some GRBs exhibit an optical plateau that consists of a phase of very shallow decay starting a few minutes after the trigger (typically 5 min in the burst rest frame) and lasting a few more minutes. The plateau can appear simultaneously in the optical and in the X-ray band (e.g. GRB 050801 De Pasquale et al. 2007); in some cases we observe an early re-brightening rather than a plateau; in other events a plateau appears in the optical on longer timescales, e.g. GRB 060206 (Stanek et al. 2007; Monfardini et al. 2006) with no correlation with any X-ray flattening.

Of the two GRB analyzed in this work, only GRB 060904B shows evidence of an optical plateau. Several scenarios could explain such a plateau. In the standard fireball scenario a nearly flat optical light curve (temporal decay index $\alpha = -0.25$) can be produced by the forward shock when the fireball is in the fast cooling regime with the observational frequency between the cooling frequency ν_c and the injection frequency ν_m, see Fig. 2 of Sari & Piran (1999). For GRB 060904B, this ordering of characteristic emission frequencies cannot be reconciled with the late ($t \gtrsim 5000$ s) optical-to-X-ray data. Another possibility is that the plateau is produced by a patchy jet, i.e. by a collimated fireball characterized by a non-uniform distribution of energy (Kumar & Piran 2000). In such a case we expect a large bump followed by a plateau (see Fig. 6 of Zhang et al. 2006), as we observe in GRB 060904B. However, we should then see the same behavior roughly simultaneously in all bands, which is inconsistent with GRB 060904B X-ray data. A last hypothesis for the origin of the optical plateau is that it is produced by a late energy injection in the fireball. Late energy injection can be ascribed to a long lasting central engine activity, or to a refreshed shock associated with a short living central engine that is releasing its energy with a variety of Lorentz factors (Rees & Meszaros 1998). This hypothesis was also proposed by De Pasquale et al. (2007) to explain the plateau observed simultaneously in optical and X-ray in GRB 050801. In our case, it is difficult to conclude about the presence of a simultaneous X-ray plateau, also because of the possible contamination by internal shock emission.

We observe a large optical plateau when a very large X-ray flare is observed (GRB 060904B) and no plateau when there is no X-flare (GRB 070420). There are not enough observations from other GRBs to confirm this point but this correlation must be addressed by acquiring data of early afterglows in both X-ray and optical wavelengths.

5. Conclusion

The optical emissions of GRB 060904B and GRB 070420 are found to increase from the end of the prompt phase, reaching a maximum of brightness at $t_{\rm peak} = 9.2$ min. and 3.3 min. respectively and then decreasing. GRB 060904B presents a large optical plateau and a huge X-ray flare. We argue that the huge X-flare occurring near $t_{\rm peak}$ is produced by an extended internal engine activity. Its presence during the optical rise is only a coincidence, and is not related to the optical flare. GRB 070420 observations would support this fact because there was no X-flare during the optical peak. We have proposed that the nature of the optical plateau of GRB 060904B, while not completely elucidated, could be related to late energy injection.

Acknowledgements. B. Gendre acknowledges support from COFIN grant 2005025417. The TAROT telescope has been funded by the *Centre National de la Recherche Scientifique* (CNRS), *Institut National des Sciences de l'Univers* (INSU) and the Carlsberg Fundation. It has been built with the support of the *Division Technique* of INSU. We thank the technical staff contributing to the TAROT project: G. Buchholtz, J. Eysseric, M. Merzougui, C. Pollas, and P. & Y. Richaud. We thank E. Rykoff who provides some images of ROTSE-III and A. Kann who suggested some useful corrections. S. Cutini, B. Preger & G. Stratta acknowledge support of ASI contract 1/024/05/0.

References

Akerlof, C., Balsano, R., Barthelmy, S., Bloch, J., et al. 1999, Nature, 398, 400
Berger, E., Kulkarni, S. R., Fox, D. B., et al. 2005, ApJ, 634, 501
Boër, M., Atteia, J. L., Damerdji, Y., et al. 2006, ApJ, 638, L71
Bringer, M., Boër, M., Peignot, C., et al. 2001, Exper. Astrophys, 12, 34
Burrows, D. N., Falcone, A., Chincarini, G., et al. 2007, Philos. Trans. A, accepted [arXiv:astro-ph/0701046]
Chincarini, G., Moretti, A., Romano, P., et al. 2007, ApJ, submitted [arXiv:astro-ph/0702371]
Cobb, B. E., & Bailyn, C. D. 2007, GCNC, 5525
Costa, E., Frontera, F., Heise, J., et al. 1997, Nature, 387, 783
D'Avanzo, P., Antonelli, L. A., Calzoletti, L., et al. 2007, GCNC, 6331
de Pasquale, M., Piro, L., Gendre, B. 2006, A&A, 455, 813
de Pasquale, M., Oates, S. R., Page, M. J., et al. 2007, MNRAS, submitted [arXiv:astro-ph/0703447]
Fox, D. 2005, in Proc. Gamma Ray Bursts in the Swift Era, ed. S. Holt, N. Geherels, & J. Nousek, AIPC
Gehrels, N., Chincarini, G., Giommi, P., et al. 2004, ApJ, 611, 1005
Gendre, B., Corsi, A., & Piro, L. 2006, A&A, 455, 803
Godet, O., & Sakamoto, T. 2007, GCNC, 6598
Granot, J., Panaitescu, A., Kumar, P., et al. 2002, ApJ, 570, L61
Grupe, D., Barthelmy, S. D., Chester, M. M., et al. 2006, GCNC, 5505
Falcone, A. D., Burrows, D. N., Lazzati, D., et al. 2006, ApJ, 641, 1010
Fugazza, D., et al. 2006, GCNC, 5513
Immler, S., Marshall, F. E., Holland, S. T., et al. 2007, GCNC, 6336
Kann, A., Klose, S. Zhang, B., et al. 2008, ApJ, submitted, [arXiv:0712.2186]
Klotz, A., Boër, M., & Atteia, J. L. 2005, GCNC, 3473
Klotz, A., Boer, M., Atteia, J. L., et al. 2006a, GCNC, 5508
Klotz, A., Gendre, B., Stratta, G., et al. 2006b, A&A, 451, L39
Kobayashi, S., & Zhang, B. 2007, ApJ, 655, 973
Kumar, P., & Piran, T. 2000, ApJ, 532, 286
Markwardt, C., Barbier, L., Barthelmy, S. D., et al. 2006, GCNC, 5520
Molinari, E., Vergani, S. D., Malesani, D., et al. 2007, A&A, 469, L13
Monfardini, A., Kobayashi, S., Guidorzi, C., et al. 2006, ApJ, 648, 1125
O'Brien, P. T., Willingale, R., & Osborne, J. 2006, ApJ, 647, 1213
Pélangeon, A. & Atteia, J.-L. 2007, GCNC, 6345
Perna, R., & Loeb, A. 1998, ApJ, 501, 467
Rees, M., & Meszaros, P. 1998, ApJ, 496, L1
Romano, P., Campana, S., & Chincarini, G. 2006, A&A, 456, 917
Roming, P., Schlady, P., Fox, D., et al. 2006, ApJ, 652, 1416
Rykoff, E. S., Yost, S. A., Krimm, H. A., et al. 2005, ApJ, 631, L121
Rykoff, E. S., Rykoff, E. S., Rujopakarn, W., Yuan, F. et al., 2006, GCNC, 5504
Sari, R., & Piran, T. 1999, ApJ, 520, 641
Sari, R., Piran, T., & Narayan, R. 1998, ApJ, 497, L17
Schlegel, D. J., Finkbeiner, D. P., & Davis, M. 1998, ApJ, 500, 525
Simon, V., Hudec, R., Pizzichini, G., et al. 2001, A&A, 366, 110
Stamatikos, M., Burrows, D. N., Cusumano, G., et al. 2007a, GCNC, 6330
Stamatikos, M., et al. 2007b, GCN-Report-48.1
Stanek, K. Z., Dai, X., Prieto, J. L., et al. 2006, ApJ, 654, L21
Stratta, G., Perri, M., Burrows, D. N., et al. 2007, GCNC, 6337
Tam, P. H., Pun, C. S. J., Huang, Y. F., et al. 2005, New Astron., 10, 535
Vestrand, W. T, Wozniak, P. R., Wren, J. A., et al. 2006, Nature, 442, 172
Wijers, R. A., & Galama, T. J. 1999, ApJ, 523, 177
Willingale, R., O'Brien, P. T., Osborne, J. P., et al. 2007, ApJ, 662, 1093
Wozniak, P. R., Vestrand, W. T., Wren, J. A., et al. 2006, ApJ, 642, L99
Wu, X. F., Dai, Z. G., Huang, Y. F., et al. 2003, MNRAS, 342, 1131
Zhang, B., & Meszaros, P. 2004, Int. J. Mod. Phys., A19, 2385
Zhang, B., Kobayashi, S., & Meszaros, P. 2003, ApJ, 595, 950
Zhang, B., Fan, Y. Z., & Dyks, J. 2006, ApJ, 642, 354